A Short-Term Energy Storage System for Voltage Quality Improvement in Distributed Wind Power

Moataz Ammar, *Student Member, IEEE*, and Géza Joós, *Fellow, IEEE*

***Abstract*—Wind power (WP) penetration in weak distribution networks is associated with adverse impacts on voltage quality. The installation of an energy storage system (ESS) is a possible voltage quality remedy in such milieus. This paper proposes a supercapacitor ESS for alleviation of voltage flicker resulting from WP integration. The proposed ESS control and management are tailored to that purpose such that the ESS offsets the flicker-producing fluctuations in the generated WP. The proposed power sizing of the ESS is defined by the estimated turbulence intensity and wind speed average at the installation site. A 2 MW wind generator of the doubly fed induction generator type is employed as a source of WP and simulations are conducted on a simplified test system, as well as a detailed 25 kV distribution network on which results are compared with acknowledged reactive power flicker mitigation approaches and verified by prototyping in a real-time simulation platform. The flicker measurement procedure is conducted per IEC Standard 61000-4-15.**

***Index Terms*—Distributed generation, energy storage, flicker, power quality, real-time simulation, storage control, supercapacitor, wind power (WP).**

I. Introduction

THE INCREASED penetration of wind power (WP) in weak distribution networks is challenged by capacity constraints imposed by power quality dictated criteria. More specifically, a major concern in distribution networks is voltage quality that experiences deterioration after WP connection due to the fluctuating nature of the generated active power. From a voltage quality perspective, WP fluctuations occur in two frequency ranges: 1) low-frequency range prompting changes in the steady-state voltage level; and 2) high-frequency range resulting in a flicker contribution. This body of work deals with the latter.

Flicker emission of a wind generator (WG) refers to the dynamic voltage changes occurring in the range of 0.05–42 Hz in 120 V/60 Hz systems as a result of the interconnection of the WG to the grid. The flicker emission stems from sources detailed in [1] and incorporated in the WG model in this paper.

Conventional mitigation of WP flicker severity is achieved by control of the reactive power flow to counteract the active WP fluctuations voltage impacts either through control of the WG converters or the use of a flexible ac transmission system (FACTS) device [2], [3]. Yet, the use of reactive power is limited by its availability [4], [5], the grid codes limitations on WGs reactive power control capability [6] and is highly restrained by the network reactance-to-resistance (X/R) ratio [1], [7] that are all decisive factors in determining the feasibility of reactive power control as a flicker mitigation approach.

Bearing in mind the high dependence of flicker severity on the network X/R ratio and the power factor setting of the flicker source as explained in [8] and [9], active power smoothing provides a flicker-mitigation solution that is independent of the network impedance as well as the desired renewable generator reactive power behavior. Active power fluctuations smoothing as a flicker mitigation solution was particularly studied in [7] and [10]. In [7], the dc link of the fully rated converter synchronous generator was used as a storage unit and in [10], the pitch control scheme of the doubly fed induction generator (DFIG) wind turbine was modified to counteract the active power dips by maintaining a reserve margin for active power increase by the turbine blades. The limitations of the former can be seen in the limited energy storage capacity the machine dc link can provide and the latter necessitates a sacrifice of the energy captured by the wind turbine and both techniques require distributed controls at each individual WG in a wind farm. Due to the outlined limitations, the aforementioned works only targeted the tower shadow fraction of the flicker-producing active power fluctuations. The flicker contribution from that fraction is deemed highly alleviated by the contemporary WG variable speed control [11] rendering the wind speed fluctuations the major source of flicker emission.

With respect to the use of a short-term energy storage system (ESS) in combination with intermittent-resource renewable energy, the works in [12]–[16] signified the effectiveness of flywheel-based and supercapacitor-based ESSs in output power leveling in very short time frames. Particularly, the works in [13]–[15] proposed a hybrid long-term (battery-based)/short-term (supercapacitor-based) ESS to smooth the WP fluctuations that are faster than the response time of the long-term battery unit. The presence of the supercapacitor unit was shown by a week-long study to remarkably extend the life time of the battery unit [15]. Yet, the question of necessary controls, sizing foundation, and physical need for the short-term ESS from a voltage quality perspective was yet to be posed as no power quality benchmark assessment was in question.

This paper complements the aforementioned studies by the following contributions: 1) proposing a combined control/management algorithm for a supercapacitor-based short-term ESS to allay the WP short-term power quality concern of voltage flicker; and 2) proposing an ESS power sizing methodology as a function of the wind speed average and turbulence intensity

Manuscript received February 28, 2014; revised August 9, 2014; accepted September 16, 2014. This work was supported in part by the Natural Sciences and Engineering Research Council of Canada under a grant from the Wind Energy Strategic Network. Paper no. TEC-00141-2014.

The authors are with the Department of Electrical and Computer Engineering, McGill University, Montréal, QC H3A 2A7, Canada (e-mail: moataz.ammar@mail.mcgill.ca; geza.joos@mcgill.ca).

Color versions of one or more of the figures in this paper are available online at http://ieeexplore.ieee.org.

Digital Object Identifier 10.1109/TEC.2014.2360071

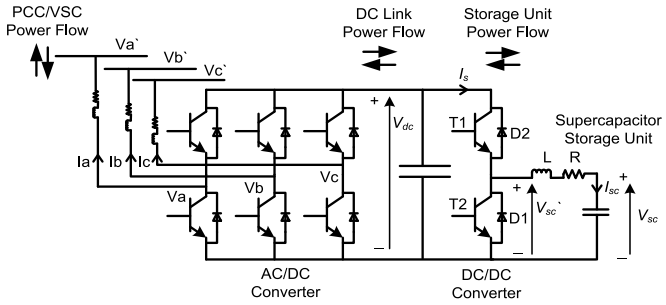

Fig. 1. Employed ESS configuration.

at the installation site. This paper concludes the results by deducing a network-equivalent-based foundation for determining the superior performance that the ESS can present over the currently adopted reactive-power-based flicker mitigation approaches.

The short-term energy sizing in the time frame of concern was done arbitrarily in the works of Abbey *et al.* [17] and Esmaili *et al.* [18] and based on an operational requirement (area below the voltage ride-through curve of the WG) in [14]. This paper adopts a methodology similar to that adopted in [14] by defining a flicker-based operational requirement (ability to store the ESS rated power for the length of the longest flicker-producing WP change).

The IEC flickermeter described in [19] is employed for flicker measurement and flicker measurements are conducted in accordance with [20] with the short-term flicker index "P_{st}" being the comparison benchmark.

II. Storage System Configuration

A. Centralized Versus Distributed Topology

Contemporary WGs are typically featured either as DFIGs or fully rated converter synchronous generators. In the fully rated converter WGs, the total WP generation traverses the fully rated converter. Conversely, the converter is rated at 20–30% of the machine rating in DFIGs. Therefore, if storage is to be connected to the machine converter dc link as in [14] and [21], converter-imposed size limitations are placed on the storage unit in case of the DFIG (20–30% of machine rating). The grouping effect and consequent reduction in power rating in multi-WG assemblies is also an advantage that centralized storage can capitalize on. Considering the previous factors, a centralized ESS is assumed for generalization purposes and two power electronic converters are employed: an ac/dc converter and a dc/dc converter (see Fig. 1).

B. AC/DC Voltage-Source Converter (VSC)

The control of the VSC is done in decoupled two-coordinate *dq* frame such that active and reactive powers are controlled independently. The basic equations describing the control action were studied extensively in literature and can be found in [22]. The VSC is controlled such that a constant dc-link voltage is maintained with the dc/dc converter assuming control of the storage unit power flow.

C. DC/DC Converter

A two-quadrant converter controls the flow of power from and to the storage unit. When switch T1 (see Fig. 1) is ON, the dc-link voltage is imposed on the storage unit branch and the flow of power is from the point of common coupling (PCC) to the storage unit, while if T2 is ON, the current reverses direction and the voltage across the storage unit branch is zero. If switch T2 is switched off, the current flowing in the switch is conducted through D2 until it drops to zero transferring power from the storage unit to the PCC. The average voltage across the storage unit branch and the storage unit current is governed by

$$V'_{\mathrm{sc}} = DV_{\mathrm{dc}} \tag{1}$$

$$I_{\mathrm{sc}} = \frac{I_s}{D} \tag{2}$$

where V'_{sc} is the average storage branch voltage, D is the duty cycle, V_{dc} is the dc-link voltage, I_{sc} is the supercapacitor current, and I_s is the average input current to the dc/dc converter. Due to the high computational burden of the required P_{st}-calculation 10-min simulation runs, (1) and (2) are used to link the dc/dc converter to the dc link in an average switching model in a subset of the presented results.

III. Storage Sizing Methodology

A. WP Flicker-Producing Content

WP flicker-producing fluctuations can be classified either as turbine-dimensions-dependent 3p torque oscillations or impacts of wind speed fluctuations. The amplitude of the 3p torque oscillations is a function of the wind turbine mechanical design (tower height, tower radius, etc. [23]) rendering it difficult to quantify without precise knowledge of the wind turbine detailed specifications and the flicker impact is lower than that of wind speed variations under contemporary WG speed control. The mathematical model of the 3p torque oscillations based on the work of Dolan and Lehn [23] is provided in Appendix A. The frequency of the oscillations depends on the rotational speed of the wind turbine and hence to properly model its impact as the WG speed changes, the raw wind speed data were coupled to the rotational speed of the turbine by the mathematical model to correctly estimate the position of the blades.

A comparison between the impacts of the two flicker-producing components on the active power generated by the WG is demonstrated by Fig. 2. Fig. 2 demonstrates the power spectral density (PSD) of both the wind speed data and the WG active power output with and without the inclusion of the 3p torques oscillations in the wind turbine model. As can be seen from Fig. 2(b) and with the aid of the dashed horizontal lines, the amplitude of active power fluctuations due to the 3p torque oscillations is smaller than that of the wind speed variations above 0.05 Hz and hence a flicker mitigation scheme based on the 3p torque oscillations will result in only partial alleviation of the flicker severity [7], [10]. The amplitude of the short-term WP fluctuations due to the wind speed variations can rather be attributed to the WP installation site. More specifically, by knowledge of the average wind speed (determined from

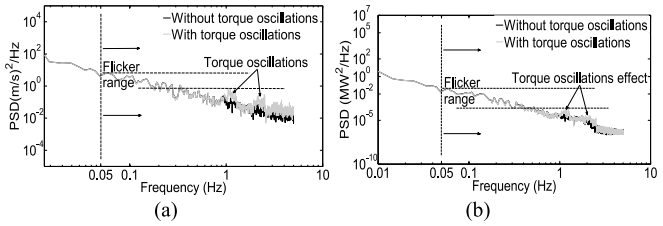

Fig. 2. Impact of the 3p torque oscillations on the output power of a WG: (a) wind speed data PSD with and without the 3p toque oscillations effect and (b) output power PSD with and without the 3p toque oscillations effect (10 m/s, 2 MW DFIG).

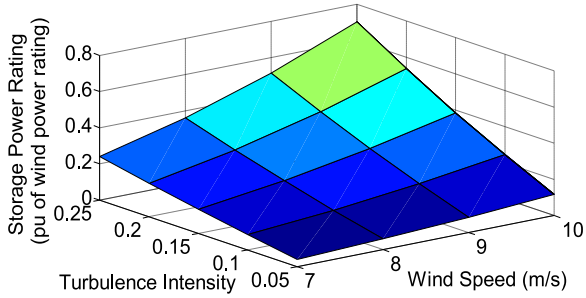

Fig. 3. Proposed storage power rating as a function of wind speed average and wind turbulence intensity (2 MW DFIG).

historical short-term wind data) and the wind turbulence intensity (a function of the installation site terrain), an estimation of the likely magnitude variations in wind speed can be derived and a translation into WP output changes can define the ESS power rating.

B. Power Sizing

The relation between the output power of a WG and wind speed at the turbine blades is governed by (3) which can be expressed as (4) in the maximum power point tracking range (below rated wind speed at constant power coefficient). This is the range most important to flicker studies, as the pitch control is reported to help alleviate the flicker severity [2]

$$P_w = \frac{\rho}{2} C_p(\beta, \lambda) A v^3 \tag{3}$$

$$P_w = K v^3, \qquad K = \frac{P_{\text{rated}}}{v_{\text{rated}}^3} \tag{4}$$

where P_w is the generated WG power, ρ is the air density, C_p is the power coefficient, β is the blade pitch angle, λ is the tip-speed ratio, A is the area swept by the turbine blades, v is the instantaneous wind speed, P_{rated} is the rated WG power, and v_{rated} is the rated wind speed.

For any change in wind speed, the postchange wind speed value (v_{new}) can be expressed in terms of the prechange value (v_{old}) and the magnitude of the change (Δv), (5). Similarly, the WP generation can be expressed in terms of the prechange value (P_{old}), postchange value (P_{new}), and magnitude of change in WP output (ΔP) as in (6) and an expression for the magnitude of change in WP can be written in terms of the wind speed change as in (7)

$$v_{\text{new}} = v_{\text{old}} + \Delta v \tag{5}$$

$$P_{\text{new}} = P_{\text{old}} + \Delta P \tag{6}$$

$$K v_{\text{new}}^3 = K v_{\text{old}}^3 + KM, \quad M = v_{\text{new}}^3 - v_{\text{old}}^3. \tag{7}$$

The term KM in (7) represents the magnitude of change in WP (ΔP) that needs to be offset should it occur at a flicker-producing frequency. In order to quantify the value of M in (7) and hence the likely magnitude changes in WP, the turbulence intensity at the installation site and the average wind speed are utilized. Wind turbulence is linked to the average wind speed by the standard deviation σ (8) and the standard deviation by its definition signifies the magnitude of likely deviations of a set of data from its average value. A deviation from the average wind speed value is thus likely to be $\pm\sigma$ of the recorded wind data and (9) can be used to describe the postchange wind speed value

$$t_{\text{ur}} = \frac{\sigma}{\bar{v}} \tag{8}$$

$$v_{\text{new}} = \bar{v} \mp t_{\text{ur}}\, \bar{v} \tag{9}$$

where t_{ur} is the wind speed turbulence intensity and $\bar{v}$ is the average wind speed. M as expressed in (7) can either be a positive or a negative value, but given the cubic exponent effect, a higher magnitude change in WP is seen for a positive change in v ($\Delta v = +t_{\text{ur}}\bar{v}$). Thus, the likely magnitude increase in wind speed is used to define the storage unit power rating.

With $\bar{v}$ being the reference wind speed around which changes are to be offset by storage charging and discharging, the value of M can be determined by (10) and the power rating of the storage unit calculated accordingly in terms of the installed WG rating, average wind speed, and turbulence intensity by (11)

$$M = (\bar{v} + t_{\text{ur}} * \bar{v})^3 - \bar{v}^3 \tag{10}$$

$$P_{\text{res}} = KM = \frac{P_{\text{rated}}}{v_{\text{rated}}^3} \left(t_{\text{ur}} * \bar{v}^3 \left(3 + 3t_{\text{ur}} + t_{\text{tu}}^2\right)\right) \tag{11}$$

where P_{res} is the power rating of the storage unit.

The storage unit power rating according to the proposed methodology is plotted in Fig. 3 as a function of the average wind speed and the turbulence intensity for the test 2 MW DFIG.

It is seen that the higher the wind speed average and the higher the turbulence intensity, the higher the required storage unit power rating. This is in line with WP flicker severity behavior that increases in intensity as both wind speed and turbulence intensity increase.

C. Energy Sizing

In terms of long-term ESSs energy sizing, optimization studies are typically carried out given a wind farm output scheduling scheme, daily forecasted wind profiles and a minimization of a cost function [24], [25]. Energy sizing optimization in that case is seen in light of the network load profile variations and consequent wind farm dispatch commands. In case of the short-term ESS studied in this paper, the load profile is constant and an optimal energy sizing for the ESS requires a precise analysis of the

higher frequency spectrum of wind speed data measured over extended time periods (months as done in [24] for the lower frequency spectrum) or by employing a mathematical time-domain representation of the wind speed profile in the short-term frame of study (order of seconds), but no standard mathematical model is agreed upon to describe the time dependence of the short-term fluctuations [26], [27]. Thus and in order to release the energy sizing of the short-term ESS from the wind speed modeling dependence and given that the economical concern in the 10-min frame is allayed [28], the short-term energy sizing has previously been done empirically as in [15], arbitrarily as in [12], [17], [18] or operational requirements were set forth as criteria to define the maximum energy storage capacity as in [14].

A combination of the two approaches utilized in [14] and [15] is employed in this paper. First, an operational requirement defines the storage energy rating $E_{\rm res}$ by the ability of the ESS to store its rated power $P_{\rm res}$ under the longest possible flicker-producing change at a frequency of 0.05 Hz and a duration of 20 s. Second, a parametric study is carried out by reduction of the ESS energy rating to observe $P_{\rm st}$ sensitivity to the rating changes.

IV. Storage Unit Control Algorithm

The proposed control for the dc/dc converter is realized in two levels: 1) a level at which the storage duty cycle is controlled (current control loop); and 2) a level at which the storage unit power consumption is controlled (power control loop).

A. Current Control Loop

A current control loop acts on the dc/dc converter switches to track the supercapacitor reference current setting. The supercapacitor is represented by a capacitance and a series resistor as done in [13] and [21] and is discharged through an inductor. By considering that representation and the switching states of the dc/dc converter of Fig. 1, the transfer function of (12) represents the duty cycle–current relationship or the controlled plant for the current control loop

$$P_1(s) = \frac{\Delta i_{\rm sc}(s)}{\Delta d(s)} = \frac{V_{\rm dc} C s}{LCs^2 + RCs + 1} \tag{12}$$

where $\Delta i_{\rm sc}$, Δd are small changes in the storage branch current and duty cycle, respectively, C is the supercapacitor capacitance, R is its series resistance, and L is the discharging inductor inductance. The characteristic design equation in that case for the current control loop is described by

$$1 + {\rm PWM}_{\rm gain} P_1(s) = 0 \tag{13}$$

where ${\rm PWM}_{\rm gain}$ is the gain introduced by the PWM switching. The current control loop transfer function including the current controller $C_1(s)$is of the form of

$$T_1(s) = \frac{C_1(s){\rm PWM}_{\rm gain} P_1(s)}{1 + C_1(s){\rm PWM}_{\rm gain} P_1(s)}. \tag{14}$$

The current control loop responds to a current reference set by an outer control loop (power control loop) whose controlled plant and characteristic equation are defined by a simultaneous flicker mitigation and storage management control scheme.

B. Power Control Loop

The active power command to the storage unit is formulated such that two purposes are fulfilled: 1) offsetting undesired WP fluctuations at the PCC and is achieved by a flicker power command $P_{\rm flicker}$; and 2) maintaining a minimum level of stored energy in the unit to allow the sought offsetting and is achieved by a management charge/discharge power command $P_{\rm char-disch}$.

1) Flicker Power Command: $P_{\rm flicker}$ is obtained from the measured P_w by means of a high-pass filter with a time constant τ_1 (3.18 s) presenting a cut-off frequency of 0.05 Hz (start of the flickering range)

$$P_{\rm flicker}(s) = P_w(s)\left(\frac{\tau_1 s}{1 + \tau_1 s}\right). \tag{15}$$

2) Management Power Command: $P_{\rm char-disch}$ is a storage management command in which changes should occur at a frequency below the start of the flickering range providing control to the storage unit state of charge (SoC) and avoiding interference with $P_{\rm flicker}$ and presenting no flicker contribution. In order to generate $P_{\rm char-disch}$, a threshold supercapacitor voltage $V_{\rm scthreshold}$ serves as a reference point to the management scheme to constantly maintain a corresponding level of energy $E_{\rm scthreshold}$ in the storage unit according to (16). $E_{\rm scthreshold}$ and therefore $V_{\rm scthreshold}$ can be defined by the ratio of a likely positive WP change (energy to be charged) to a likely negative WP change (energy to be discharged)

$$SoC_{\rm scthreshold} = \frac{E_{\rm scthreshold}}{E_{\rm res}} = \frac{V^2_{\rm scthreshold} - V^2_{\rm min}}{V^2_{\rm max} - V^2_{\rm min}} \tag{16}$$

where $V_{\rm max}$ and $V_{\rm min}$ are the maximum and minimum operating voltages of the installed supercapacitor, respectively. A management frame of 40 s is found appropriate allowing changes of a maximum frequency of 0.025 Hz to be seen in $P_{\rm char-disch}$ utilizing a low-pass filter of a time constant τ_2 (6.37 s)

$$P_{\rm char-disch}(s) = P_{\rm mang}(s)\left(\frac{1}{1 + \tau_2 s}\right) \tag{17}$$

where $P_{\rm mang}(t) = \frac{0.5 * C * (V^2_{\rm sc}(t) - V^2_{\rm scthreshold})}{40}$, and $V_{\rm sc}(t)$ is the instantaneous voltage of the supercapacitor unit. The characteristic design equation for the power controller was obtained from small-signal analysis and is described by

$$1 + H_2(s)T_1(s) = 0 \tag{18}$$

where $H_2\,(s)$ represents the equivalent active power feedback loop containing both the measurement and management feedback signals (19). The detailed small-signal model is shown in Fig. 4 and the system control design is illustrated by bode plots for the base study case in Section V

$$H_2(s) = V_{\rm sc}\left(1 + \frac{1}{40s\,(1 + \tau_2 s)}\right) + \frac{I_{\rm sc}}{sC} \tag{19}$$

where $V_{\rm sc}$ and $I_{\rm sc}$ are the supercapacitor voltage and current values at which the controllers parameters are designed.

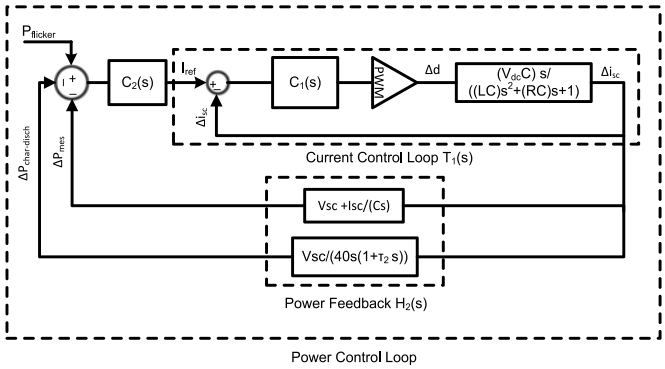

Fig. 4. Small-signal block diagram for the supercapacitor control loops.

C. Controller Limits and Design Procedure

A commercial supercapacitor cell [13] is the basis of the presented data. The rated voltage of the cell is 400 V with a capacitance of 0.58 F and an equivalent series resistance of 0.6 Ω. The different parameters of the storage unit and accompanying control limits are specified as follows.

1) *Voltage Limits:* The maximum voltage is determined by the dc-link voltage $V_{\rm dc}$ and the minimum voltage is controlled by the limits on the duty cycle and the converter and is determined in this work by limiting the power loss in *R* occurring at $I_{\rm max}$ to 0.1 $P_{\rm res}$.
2) *Capacitance:* The equivalent capacitance of all series and parallel cells is determined by the energy rating of the storage unit and the operating voltage limits

$$C = \frac{2E_{\rm res}}{(V_{\rm max}^2 - V_{\rm min}^2)}. \tag{20}$$

3) *Current Limits:* The maximum current $I_{\rm max}$ occurs as the rated power is delivered to the storage unit at $V_{\rm min}$ and is calculated as follows:

$$I_{\rm max} = \frac{P_{\rm res}}{V_{\rm min}}. \tag{21}$$

V. Simulation Results and Case Studies

To thoroughly verify the proposed ESS operation, the following sets of simulations were conducted: *Simulations 1*—ESS performance verification and parameter sensitivity analysis on a single 2 MW DFIG unit connected to a simplified equivalent-impedance network as a bases case, *Simulations 2*—testing of three storage-equipped wind farm integration scenarios to a detailed 25 kV North American network (WP capacities of 6, 8, and 10 MW) and *Simulations 3*—real-time prototyping of a sample subset of *Simulations 2* in a real-time simulation platform to validate the real-time performance of the ESS control algorithm. The WG unit parameters are shown in Table I.

A. Base Case (Simulations 1)

A weak distribution network is represented by its *X*/*R* ratio and short-circuit level as seen at the point of WP connection. The connection point characteristics are 25 kV voltage level,

TABLE I
WG Parameters

Parameter	Value	Unit
Power rating	2	MW
Rotor resistance	0.016	p.u.
Rotor inductance	0.16	p.u.
Stator resistance	0.023	p.u.
Stator inductance	0.18	p.u.
Generator inertia constant	0.8	s
Turbine inertia constant	4.2	s

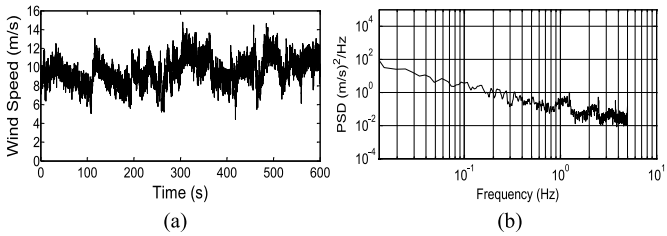

Fig. 5. Wind resource at 10 m/s and turbulence intensity of 15%: (a) time series; and (b) PSD.

TABLE II
Storage Stack Parameters

Parameter	Symbol	Value	Unit
Power rating	$P_{\rm res}$	770	kW
Energy rating	$E_{\rm res}$	4.27	kW · h
Maximum voltage	$V_{\rm max}$	1150	V
Minimum voltage	$V_{\rm min}$	345	V
Maximum current	$I_{\rm max}$	2.23	kA
Total capacitance	C	25.58	F
Threshold voltage	$V_{\rm threshold}$	790	V

30 MVA short-circuit level, and an *X*/*R* ratio of 0.5. The ESS is connected to the low-voltage side of the MV/LV transformer at 575 V. The assumed wind speed characteristics at the installation site are an average of 10 m/s and turbulence intensity of 15%. Fig. 5 shows the temporal and PSD plots of the 10-min wind speed profile applied at the turbine blades. The corresponding ESS parameters according to the proposed sizing and design procedure are shown in Table II.

The linearized small-signal control design was conducted at values of $V_{\rm dc} = 1150\,{\rm V}$, $V_{\rm sc} = V_{\rm threshold} = 790\,{\rm V}$, ${\rm PWM}_{\rm gain} = 0.5$, $I_{\rm sc} = 975$ A and rest of parameters per Table II. The intent was to determine the type of controller to be used such that the system stability can be maintained. The characteristic equation of the current control loop (13) was used to specify the current controller desired transfer function by aid of its Bode plot. It is seen from Fig. 6(a) that the open-loop transfer function for the current control loop presents an infinite gain margin and +90° phase margin and hence a pole introduced at the origin by a proportional-integral controller does not affect the system stability as long as its phase is cancelled by the introduced zero at higher frequencies. The values for the proportional and the integral controllers were set, respectively, at 2 and

he exception of pagination.

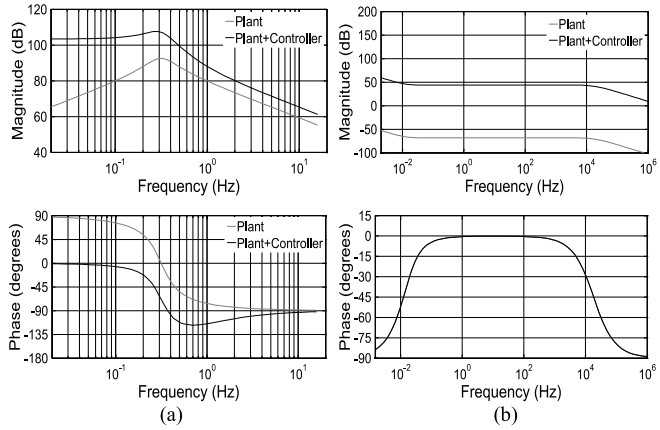

Fig. 6. Bode plots of the supercapacitor control loops: (a) current control loop; and (b) power control loop.

10 such that the phase effect of the controller pole is cancelled at a break frequency of around 5 Hz [see Fig. 6(a)]. Similarly, the characteristic equation for the power controller (18) was used to design the power loop controller. As can be seen from the Bode plot of Fig. 6(b), a proportional-integral controller with a pole at the origin results in an unstable operation by yielding a phase of –180°; a proportional controller rather maintains the loop stability under all conditions and is hence employed. A comparison of the small-signal model (used for controller design) and the large-signal model (power system) response under the proposed controllers is shown in Appendix B.

On the supercapacitor side of the ESS, the system operation is illustrated by the plots of Fig. 7 in p.u. of storage base quantities (see Table II). The corresponding operation on the VSC side (distribution network side) is shown in Fig. 8. The conclusive impact of the ESS on facilitating WP integration is seen in both the active power injected from the WG into the network and the PCC RMS voltage waveform as seen in Fig. 8(b) and (c). Figs. 7(b) and 8(a) demonstrate the change in the ESS current magnitude and direction of flow in correspondence with the flicker content in WP generation shown in Fig. 7(a). The ESS ability in eliminating a target range of frequencies in the WP generation is demonstrated by the PSD of the active power components shown in Fig. 9 at the point of connection. The ESS power consumption is shown coinciding with that of WP generation, in the absence of the ESS, in the targeted frequency range (flickering range). The presence of the ESS resulted in the elimination of a portion of the WP frequency spectrum corresponding to the flicker-producing components in the wind speed spectrum shown in Fig. 5(b) and yielded WP injection of PSD of lower amplitude in the flickering range. The ESS management power is shown to be conducted over a lower range of frequencies with negligible PSD in the flicker frequency range. This is also demonstrated by the temporal plots in Fig. 7(d) and (e) in which the storage unit discharge command is seen to respond to the level of energy content in the unit, yet with a less fluctuant profile due to the filtering effect in the management scheme. The efficacy of the proposed ESS control algorithm is seen in the alleviated flicker severity at the PCC as shown in Fig. 10

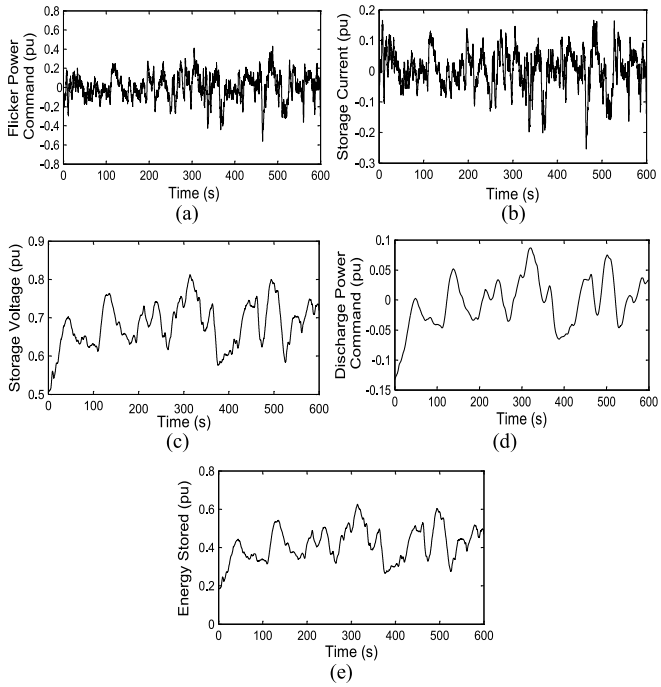

Fig. 7. ESS operation (supercapacitor side): (a) filtered flicker power command; (b) supercapacitor current; (c) supercapacitor voltage; (d) management discharge power command; and (e) energy stored in the supercapacitor unit. Units in p.u. of base quantities in Table II.

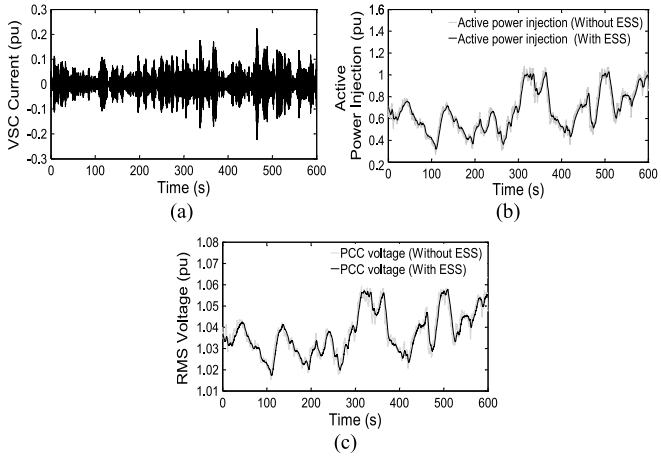

Fig. 8. ESS operation (VSC side): (a) VSC current; (b) injected active power; and (c) PCC voltage profile. Units in p.u. of WG base quantities (2 MW, 575 V).

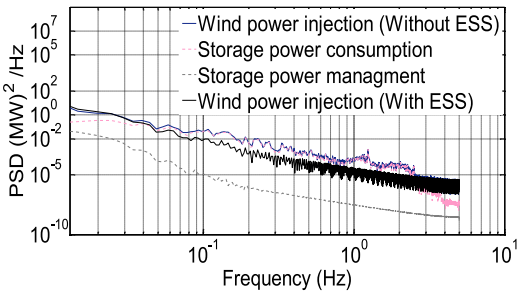

Fig. 9. PSD of active power components.

 he exception of pagination.

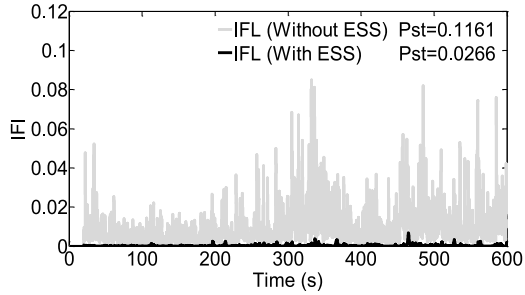

Fig. 10. IFL and P_{st} values at the PCC with and without the ESS.

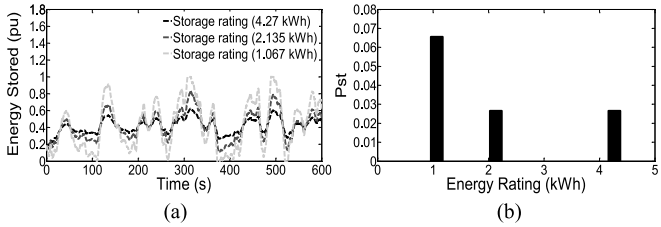

Fig. 11. P_{st} sensitivity to energy rating: (a) energy stored; and (b) P_{st} values.

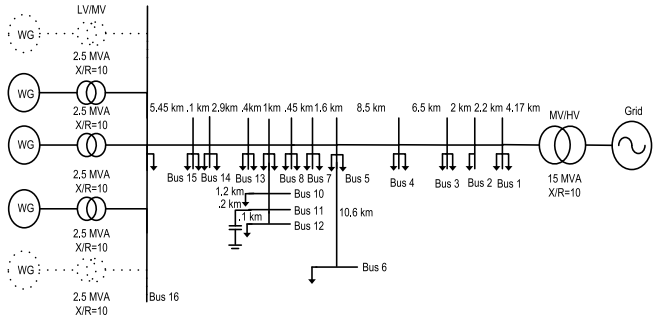

Fig. 12. Detailed 25 kV distribution network layout.

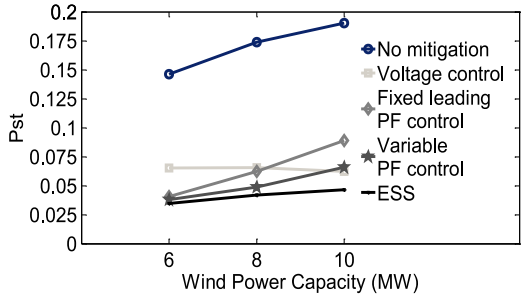

Fig. 13. P_{st} values versus WP capacity at Bus 16 of the detailed 25 kV distribution network.

in terms of instantaneous flicker level (IFL) and statistically calculated P_{st}.

A parametric study was carried out to determine the sensitivity of P_{st} to variations in storage unit energy sizing. The energy sizing of the storage unit was calculated based on a 20 s charging duration under the power rating P_{res}. This proved to be a conservative approach with a safety margin ensuring that the unit does not reach its capacity limits. Fig. 11 shows the impact of reducing that rating to half and quarter its design values (2.13 and 1.07 kW · h). It is seen that at half the design energy rating, the storage unit did not reach its limits not impacting the P_{st} values. When the rating was further reduced, the storage unit reached its limits resulting in periods of saturation and uncompensated WP changes and therefore impaired flicker mitigation and higher P_{st} values.

B. Detailed Distribution Network (Simulations 2)

To help identify the need for a short-term ESS in cases where reactive power control is a potential flicker mitigation solution, storage-equipped WP generation was compared to three salient flicker mitigation alternatives reported in the literature [1], [2], namely: 1) voltage control; 2) fixed leading power factor control (continuous absorption of reactive power by the WGs); and 3) variable power factor control (steady-state unity power factor for low-frequency active power changes, and nonunity for higher frequency flicker-producing active power changes). The measurements were conducted at Bus 16 (29 MVA short-circuit level) of the detailed distribution network shown in Fig. 12.

The network has three types of distribution conductors of *X/R* ratios of 3.4, 1.3841, and 0.899. The MV/HV transformer is rated at 15 MVA and has an *X/R* ratio of 10 and the LV/MV transformers are rated at 2.5 MVA and have an *X/R* ratio of 10 each. The number of WGs was increased by one unit at a time from 3 to 5 (6–10 MW) creating three short-circuit capacity ratios (5, 3.6, and 3). The P_{st} values were calculated for each case and plotted in Fig. 13 versus the WP capacity.

The prime observation regarding Fig. 13 is that the mitigation capability of one scheme with respect to another changed by change of WP capacity. Energy storage provided the lowest P_{st} values under all scenarios and was approached by fixed leading and variable power factor control as the WP capacity decreased. The ESS and voltage control were the least sensitive approaches to WP capacity changes with negligible variation in the resulting P_{st} values.

An explanation for the shown trends is traced by analysis of the equivalent two-bus system with Bus 16 being the sending end with voltage magnitude V_{se}, V_g being the receiving end constant voltage, δ being the voltage vectors angle difference, *P* and *Q* the active and reactive power flows at Bus 16 flowing into the network, and *R* and *X* the resistance and reactance of the equivalent impedance seen at Bus 16, respectively. Equations (22) and (23), respectively, represent the real and imaginary parts of the power flow equation for such system

$$V_{\mathrm{se}}(V_{\mathrm{se}} - V_g \cos\delta) = (PR + QX) \tag{22}$$

$$V_g V_{\mathrm{se}} \sin\delta = (PX - QR). \tag{23}$$

As δ diminishes to approach negligible values as assumed in distribution networks, (22) is approximated by (24) to represent the change in voltage magnitude between the two buses. Equation (24) is the basis of voltage changes compensation by power factor control at the PCC (fixed leading power factor and

he exception of pagination.

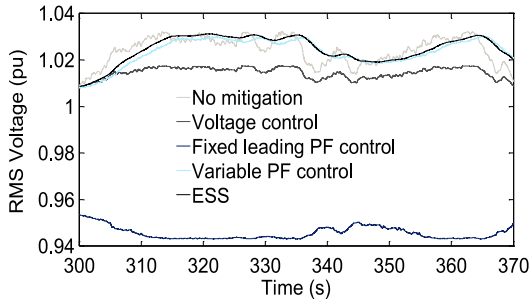

Fig. 14. Short-term profile of Bus 16 voltage for different flicker mitigation techniques (6 MW rating scenario).

variable power factor control)

$$(V_{\rm se} - V_g) \approx \frac{(PR + QX)}{V_{\rm se}}. \tag{24}$$

In fixed leading power factor, reactive power compensates the entire WP generation, while in variable power factor control, (24) is split into two spectra: one outside the flicker frequency range (average WP output and slow changes of high magnitude) and the other covering the flicker range (faster WP changes with lower magnitude), thus treating the voltage level and flicker independently. Bearing in mind that the total WP generation [see Fig. 8(b)] is essentially a nonflicker-producing active power generation level over which a flicker-producing content is superimposed [see Fig 7(a)] and assuming the total WP generation to be P_1, and the amplitude of a flicker-producing change to be P_2, then $P_1 \geq P_2$. Therefore, when the flicker-component is treated independently, a smaller value of δ is involved in the approximation of (24) as compared to the case of leading power factor increasing the validity of (24) and leading to variable power factor maintaining a superiority over fixed leading power factor for all cases and both schemes having a decreasing flicker-mitigation capacity as δ increases. δ increases by both the increase of active WP injection as well as the WG absorption of reactive power. The mitigation capability of the ESS was approached by mitigation techniques based on (24) as δ approached zero and higher accuracy of (24) (3 units case where $\delta = 1.02$ under leading power factor control and increases to 7.09° for the 5 units case). The $P_{\rm st}$ values under voltage control and the ESS are the least sensitive to WP size changes due to the voltage feedback nature of the voltage control process (nonexisting in power factor control) and the independence of the ESS control of the distribution line parameters. The mitigation capability of both methods is expected to be sensitive to the voltage controller gain (defined voltage/reactive power droop characteristics) and the ESS control gains. A sensitivity analysis of the impact of controller gains is left for future investigation. A short-term voltage profile under all mitigation alternatives for the case of 6 MW WP rating is shown in Fig. 14.

C. Validation by Real-Time Prototyping (Simulations 3)

The WP integration scenario of three wind turbines (6 MW) was used as a sample case for real-time performance validation

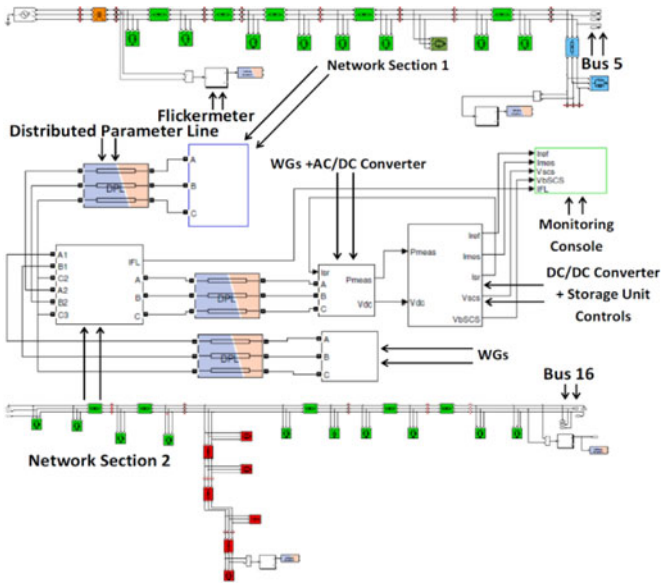

Fig. 15. System real-time prototype layout (ESS case).

of the proposed ESS control algorithm as well as the behavior of the reactive power flicker mitigation schemes. The prototype power system was developed according to the real-time digital simulation software rules resulting in a set of subsystems each simulated on a processor core of its own on the real-time simulator.

With respect to Fig. 15 and abiding by the limitations on the number of elements that can be processed in one subsystem, the WP-distribution-network power system was constructed as follows: 1) distribution network: two subsystems, the master subsystem and a slave subsystem; 2) WGs: two slave subsystems; 3) WGs reactive power controls: one slave subsystem; and 4) ESS dc/dc converter control and management algorithm: one slave subsystem.

The online flickermeters were placed at the buses of concern in the subsystems containing the distribution network elements. Three studies were performed to validate the ESS real-time performance: 1) performance of the ESS control algorithm; 2) flicker profile study across the network buses with and without the ESS; and 3) a comparison of the flicker measurements with the ESS and the reactive power control schemes as measured at the PCC (Bus 16).

1) ESS Control Real-Time Performance: The ESS control performance was observed by recording the ESS active power components as well as the tracking error fed to the power controller. Similarly, the current measurements were performed in the supercapacitor branch as well as one phase of the VSC; the results are shown in Fig. 16.

In Fig. 16(a), the flicker power command, the discharge power command, and the measured storage power consumption are shown. The tracking error fed to the power controller is shown in Fig. 16(b). The impact of the storage control algorithm on the current withdrawn by the ESS is demonstrated by the short-term plots of the ESS VSC phase current and the supercapacitor branch current in Fig. 16(c) and (d), respectively.

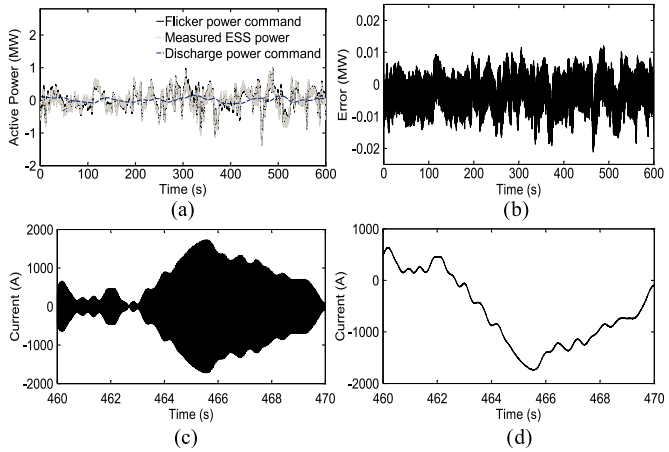

Fig. 16. ESS control real-time performance (real-time prototype, 6 MW rating scenario): (a) ESS power commands; (b) ESS power tracking error; (c) short-term ESS VSC phase current; and (d) short-term supercapacitor current.

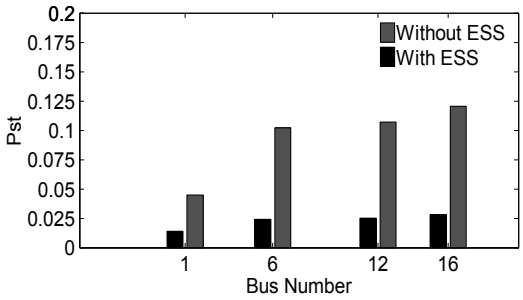

Fig. 17. Network flicker profile (real-time prototype, 6 MW rating scenario).

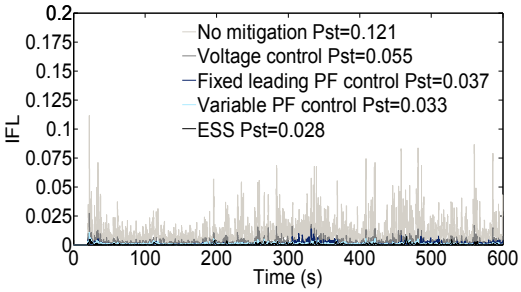

Fig. 18. IFL and P_{st} values at Bus 16 under different flicker mitigation alternatives (real-time prototype, 6 MW rating scenario).

2) Network Flicker Profile: The ESS impact on alleviating the flicker severity across the distribution network was assessed by conducting flicker measurements starting at the connection bus (Bus 16) and moving further upstream to the MV/HV transformer (Bus 1).

The results are shown in Fig. 17 as conducted at four network buses. The impact of the ESS is more conspicuously seen at buses closest to the WP connection bus reducing flicker severity by as high as 77% at Bus 16 and as low as 68% at Bus 1.

3) Comparison of the Flicker Mitigation Alternatives: The flicker measurements at the PCC (Bus 16) under all the mitigation alternatives discussed in the previous section are shown in Fig. 18. From Fig. 18, it is seen that the same trend of results was obtained from the real-time prototype except that the original flicker severity without flicker mitigation is slightly lower than the original case of offline simulations. This is attributed to an inevitable variation in the network structure introduced by distributed parameter lines dictated by the rules of the real-time simulator to separate the constructed subsystems. The ESS exhibited its superior flicker mitigation performance.

VI. Conclusion

In this paper, supercapacitor energy storage was proposed as a solution to the voltage flicker problem in weak distribution networks with WP integration. It was shown that a power sizing methodology based on wind speed average and turbulence intensity is appropriate for alleviating the voltage impacts of the flicker-producing changes in the generated WP. A filtering-based control algorithm was shown effective in both alleviating the WP flicker severity and properly managing the ESS SoC. The ESS was found to have a superior flicker mitigation capability to that of the reactive power control approaches. Nevertheless, the degree of superiority that the ESS presented was shown to be tied to the connected WP capacity and approximations assumed in the power-factor-based flicker mitigation approaches. The choice of a flicker mitigation approach should thus be contemplated in light of the planned WP capacity and taking the network impedance and the operative grid code requirements into consideration.

Appendix A
3p Torque Oscillations Model

The wind speed data used in the simulations constituted of three components

$$V_{\mathrm{eq}} = V_H + V_{\mathrm{ts}} + V_{\mathrm{ws}} \tag{A.1}$$

where V_H is the raw wind time series (a 10-min window of raw wind speed data sampled at 0.1 s), V_{ts} is the impact of the cyclic tower shadow, and V_{ws} is the wind shear effect.

The mathematical model used for the torque shadow component is of the form of (A.2) and the wind shear of the form of (A.3) as proposed in [23]

$$V_{\mathrm{ts}} = \frac{\left(1+\frac{\alpha(\alpha-1)r^2}{8H^2}\right)V_H}{3r^2}\sum_{n=1}^{3}\frac{a^2}{\sin^2\theta_n}\ln\left(\frac{r^2\sin^2\theta_n}{x^2}+1\right) - \frac{2a^2r^2}{r^2\sin^2\theta_n+x^2} \tag{A.2}$$

$$V_{ws} = V_H\left(\frac{\alpha(\alpha-1)r^2}{8H^2}+\frac{\alpha(\alpha-1)(\alpha-2)r^3}{60H^3}\cos 3\theta_n\right) \tag{A.3}$$

he exception of pagination.

TABLE III
3P TORQUE OSCILLATIONS MODEL

Parameter	Symbol	Value	Unit
Hub height	H	90	m
Rotor radius	r	40	m
Tower radius	a	2	m
Distance from blade origin to tower midline	x	3	m
Wind shear exponent		0.3	–

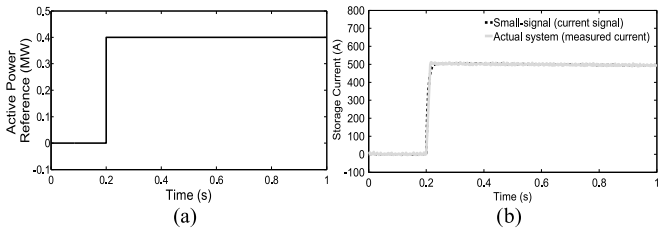

Fig. 19. Small-signal model response: (a) step change of storage active power reference; and (b) storage current signal.

where θ_n is the angle of blade n determined from the rotational speed and assuming a three-bladed wind turbine and the rest of constants and their values as per Table III.

APPENDIX B
SMALL-SIGNAL MODEL RESPONSE

The response of both the small-signal and large-signal ESS models was tested by applying a step reference change of 0.2 p.u. of the WG rating (0.4 MW) to both systems and recording the current measurements. The response is shown in Fig. 19.

REFERENCES

[1] M. Ammar and G. Joos, "The impact of distributed wind generators reactive power behavior on flicker severity," *IEEE Trans. Energy Convers.*, vol. 28, no. 2, pp. 425–433, Jun. 2013.

[2] S. Tao, C. Zhe, and F. Blaabjerg, "Flicker study on variable speed wind turbines with doubly fed induction generators," *IEEE Trans. Energy Convers.*, vol. 20, no. 4, pp. 896–905, Dec. 2005.

[3] H. Chong, A. Q. Huang, M. E. Baran, S. Bhattacharya, W. Litzenberger, L. Anderson, A. L. Johnson, and A.-A. Edris, "STATCOM impact study on the integration of a large wind farm into a weak loop power system," *IEEE Trans. Energy Convers.*, vol. 23, no. 1, pp. 226–233, Mar. 2008.

[4] A. Keane, L. F. Ochoa, E. Vittal, C. J. Dent, and G. P. Harrison, "Enhanced utilization of voltage control resources with distributed generation," *IEEE Trans. Power Syst.*, vol. 26, no. 1, pp. 252–260, Feb. 2011.

[5] M. Z. Sujod, I. Erlich, and S. Engelhardt, "Improving the reactive power capability of the DFIG-Based wind turbine during operation around the synchronous speed," *IEEE Trans. Energy Convers.*, vol. 28, no. 3, pp. 736–745, Sep. 2013.

[6] *Requirements for the Interconnection of Distributed Generation to the Hydro-Québec Medium-Voltage Distribution System*, 2009.

[7] W. Hu, Z. Chen, Y. Wang, and Z. Wang, "Flicker mitigation by active power control of variable-speed wind turbines with full-scale back-to-back power converters," *IEEE Trans. Energy Convers.*, vol. 24, no. 3, pp. 640–649, Sep. 2009.

[8] F. Sharkey, J. MacEnri, E. Bannon, M. Conlon, and K. Gaughan, "Resource-induced voltage flicker for wave energy converters- assessment tools," *IET Renew. Power Gener.*, vol. 7, no. 6, pp. 623–630, Nov. 2013.

[9] A. Blavette, D. L. O'Sullivan, R. Alcorn, T. W. Lewis, and M. G. Egan, "Impact of a medium-size wave farm on grids of different strength levels," *IEEE Trans. Power Syst.*, vol. 29, no. 2, pp. 917–923, Mar. 2014.

[10] Y. Zhang, Z. Chen, W. Hu, and M. Cheng, "Flicker mitigation by individual pitch control of variable speed wind turbines with DFIG," *IEEE Trans. Energy Convers.*, vol. 29, no. 1, pp. 20–28, Mar. 2014.

[11] H. Emanuel, M. Schellschmidt, S. Wachtel, and S. Adloff, "Power quality measurements of wind energy converters with full-scale converter according to IEC 61400–21," in *Proc. 10th Int. Elect. Power Quality Utilization Conf.*, 2009, pp. 1–7.

[12] G. O. Cimuca, C. Saudemont, B. Robyns, and M. M. Radulescu, "Control and performance evaluation of a flywheel energy storage system associated to a variable speed wind generator," *IEEE Trans. Ind. Electron.*, vol. 53, no. 4, pp. 1074–1085, Jun. 2006.

[13] L. Wei, G. Joos, and J. Belanger, "Real-time simulation of a wind turbine generator coupled with a battery supercapacitor energy storage system," *IEEE Trans. Ind. Electron.*, vol. 57, no. 4, pp. 1137–1145, Apr. 2010.

[14] C. Abbey and G. Joos, "Supercapacitor energy storage for wind energy applications," *IEEE Trans. Ind. Appl.*, vol. 43, no. 3, pp. 769–776, May/Jun. 2007.

[15] A. M. Gee, F. V. P. Robinson, and R. W. Dunn, "Analysis of battery lifetime extension in a small-scale wind-energy system using supercapacitors," *IEEE Trans. Energy Convers.*, vol. 28, no. 1, pp. 24–33, Mar. 2013.

[16] P. Thounthong, "Model based-energy control of a solar power plant with a supercapacitor for grid-independent applications," *IEEE Trans. Energy Convers.*, vol. 26, no. 4, pp. 1210–1218, Dec. 2011.

[17] C. Abbey, K. Strunz, and G. Joos, "A knowledge-based approach for control of two-level energy storage for wind energy systems," *IEEE Trans. Energy Convers.*, vol. 24, no. 2, pp. 539–547, Jun. 2009.

[18] A. Esmaili, B. Novakovic, A. Nasiri, and O. Abdel-Baqi, "A hybrid system of Li-Ion capacitors and flow battery for dynamic wind energy support," *IEEE Trans. Ind. Appl.*, vol. 49, no. 13, pp. 1649–1657, Jul./Aug. 2013.

[19] *IEEE Recommended Practice-Adoption of IEC 61000-4-15:2010 Electromagnetic Compatibility (EMC)-Testing and Measurement Techniques-Flickermeter-Functional and Design Specifications*, IEEE Standard 1453-2011, 2011.

[20] *Wind Turbine Generator Systems Part 21: Measurement and Assessment of Power Quality Characteristics of Grid Connected Wind Turbines*, IEC Standard 614000-21, 2001.

[21] L. Qu and W. Qiao, "Constant power control of DFIG wind turbines with supercapacitor energy storage," *IEEE Trans. Ind. Appl.*, vol. 47, no. 1, pp. 359–367, Jan./Feb. 2011.

[22] L. Xu, L. Yao, and C. Sasse, "Grid integration of large DFIG-based wind farms using VSC transmission," *IEEE Trans. Power Syst.*, vol. 22, no. 3, pp. 976–984, Aug. 2007.

[23] D. S. Dolan and P. W. Lehn, "Simulation model of wind turbine 3p torque oscillations due to wind shear and tower shadow," *IEEE Trans. Energy Convers.*, vol. 21, no. 3, pp. 717–724, Sep. 2006.

[24] T. K. A. Brekken, A. Yokochi, A. von Jouanne, Z. Z. Yen, H. M. Hapke, and D. A. Halamay, "Optimal energy storage sizing and control for wind power applications," *IEEE Trans. Sustain. Energy*, vol. 2, no. 1, pp. 69–77, Jan. 2011.

[25] Q. Li, S. S. Choi, Y. Yuan, and D. L. Yao, "On the determination of battery energy storage capacity and short-term power dispatch of a wind farm," *IEEE Trans. Sustain. Energy*, vol. 2, no. 2, pp. 148–158, Apr. 2011.

[26] J. G. Slootweg, S. W. H. de Haan, H. Polinder, and W. L. Kling, "General model for representing variable speed wind turbines in power system dynamic simulations," *IEEE Trans. Power Syst.*, vol. 18, no. 1, pp. 144–151, Feb. 2003.

[27] C. Nichita, D. Luca, B. Dakyo, and E. Ceanga, " Large band simulation of the wind speed for real-time wind turbine simulators," *IEEE Trans. Energy Convers.*, vol. 17, no. 4, pp. 523–529, Dec. 2002.

[28] J. Barton and D. Infield, "Energy storage and its use with intermittent renewable energy," *IEEE Trans. Energy Convers.*, vol. 19, no. 2, pp. 441–448, Jun. 2004.

 he exception of pagination.

Moataz Ammar (S'09) received the B.Eng. degree in electrical engineering from Cairo University, Giza, Egypt, in 2006, and the M.ScE. degree in electrical engineering from the University of New Brunswick, Fredericton, NB, Canada in 2009, and is currently working toward the Ph.D. degree at McGill University, Montréal, QC, Canada.

His current research interests include grid interface of renewable energy sources, energy storage, power quality, and control of distributed generation.

Géza Joós (M'82–SM'89–F'06) received the M.Eng. and Ph.D. degrees in electrical engineering from McGill University, Montréal, QC, Canada, in 1974 and 1987, respectively.

He has been a Professor at McGill University since 2001. He is involved in fundamental and applied research related to the application of high power electronics to power conversion, and the integration of distributed generation and renewable energy in electric power systems. His experience also includes employment with ABB, the University of Quebec, and Concordia University, Montréal. He has published extensively and presented numerous papers and tutorials on these topics. He has been involved in consulting activities in power electronics and power systems, and with the Centre for Energy Advancement through Technological Innovation (CEATI) in a number of assignments.

Dr. Joós is active in a number of IEEE Industry Applications Society Committees, and in the IEEE Power Engineering Society and Conseil International des Grands Réseaux Électrique (CIGRÉ) activities, and working groups dealing with power electronics and applications to distributed resources. He is a Fellow of the Canadian Academy of Engineering.